EUROPEAN ORGANIZATION FOR NUCLEAR RESEARCH

CERN-EP/98-160
6 October 1998

# CROSS-SECTIONS FOR NEUTRAL-CURRENT NEUTRINO-NUCLEUS INTERACTIONS : APPLICATIONS FOR $^{12}$C and $^{16}$O

**N. Jachowicz, S. Rombouts, K. Heyde[1] and J. Ryckebusch**

Department of Subatomic and Radiation Physics, Proeftuinstraat, 86
B-9000 Gent (Belgium)
[1]Present address : EP-ISOLDE, CERN CH-1211, Geneva 23

## Abstract

We calculate cross sections for neutral current quasi-elastic neutrino-nucleus scattering within a continuum RPA model, based on a Green's function approach. As residual interaction a Skyrme force is used. The unperturbed single particle wave functions are generated using either a Woods-Saxon potential or a Hartree-Fock calculation. These calculations have interesting applications. Neutrinos play an important role in supernova nucleosynthesis. To obtain more information about these processes, cross sections are folded with a Fermi-Dirac distribution with temperatures of approximately $10^9$ K.

(ISOLDE GENERAL)

(*Submitted for publication in Physical Review C*)

## I. INTRODUCTION

Neutrinos are extremely well-suited probes to provide detailed information about the structure and properties of the weak interaction, as they are only interacting via the weak forces. Moreover, being intrinsically polarized and coupling to the axial vector as well as to the vector part of the hadronic current, neutrinos are able to reveal other and more precise nuclear structure information than e.g. electrons do. The most important problem in extracting information from neutrino-nucleus scattering experiments remains the very small interaction cross-sections.

These restrictions become rather unimportant when considering astrophysical processes. The amount of neutrinos produced at the end of the lifetime of a massive star during the neutronization of the collapsing core of a star and its subsequent cooling, is as large as $\sim 10^{58}$, representing approximately 99% of the total released energy [1,2]. These supernova neutrinos will play an important role in explosive nucleosynthesis processes, causing a considerable transformation of the material synthesized during the hydrostatic burning phases in the life of the star.

During the last years, a large number of quasi-elastic neutrino-nucleus scattering studies have been carried out, including shell model [3], relativistic fermi gas [3,4], and RPA calculations using various forces [4–8]. Since both the LSND and the KARMEN collaboration have been measuring neutrino-nucleus scattering cross-sections on $^{12}$C [9,10], special attention was paid to the calculation of cross-sections for the reactions $^{12}C(\nu_e, e^-)X$ and $^{12}C(\nu_\mu, \mu^-)X$. Despite the theoretical and experimental efforts, no clear agreement between theory and experiment, and between the different theoretical results for the $^{12}C(\nu_\mu, \mu^-)^{12}X$ reaction could be reached [8,9,11–13]. Next to these problems, we observe that relatively few neutral-current calculations have been performed [3,5].

In the present work, we examine quasi-elastic neutral-current neutrino-nucleus reactions in an energy region relevant to explosive nucleosynthesis processes, using a continuum random phase approximation (CRPA) formalism (sect. 3). The CRPA equations are solved using a Green's function approach in which the polarization propagator is approximated by an iteration of the first-order contribution [14]. The unperturbed wave-functions are generated using either a Woods-Saxon potential or a HF-calculation using a Skyrme force. The latter approach makes self-consistent HF-RPA calculations possible. Calculations using either a Skyrme or a Landau-Migdal force must give indications about possible differences and sensitivity in methods to the residual two-body interaction used. Finally, we discuss applications for neutral-current reactions on $^{16}$O and $^{12}$C, two nuclei that are very important from an astrophysical point of view. In section 6, we discuss some aspects of neutrino nucleosynthesis and in section 7, the stability of the RPA and TDA methods, using different two-body forces in calculating the neutrino scattering cross-section, is discussed.

## II. QUASI-ELASTIC NEUTRINO SCATTERING

In the neutral-current neutrino scattering reactions, a neutrino with four-momentum $(\epsilon_i, \vec{k}_i)$ is scattered inelastically from a nucleus with initial energy and momentum $E_i$, $\vec{P}_i$. The nucleus is supposed to be spherically symmetric and in its ground state, $\mathrm{J}_i^{\pi_i} = 0^+$. After the reaction, the nucleus is left in an excited state with final parity and angular momentum

$J_f, \pi_f$. The energy transferred from neutrino to nucleus, the excitation energy of the nucleus, equals $\omega = \epsilon_i$-$\epsilon_f$ = $E_f$-$E_i$, $\epsilon_f$ and $E_f$ being the final neutrino and nuclear energy respectively. The transferred momentum is denoted by $\vec{q} = \vec{k}_i - \vec{k}_f$, $\kappa = |\vec{q}|$.

As the interaction between the neutrino and a nucleus is mediated by the weak interaction, the cross-section can be derived using Fermi's golden rule. In Born approximation, the outgoing neutrino is described by a plane wave. The density of final states $\rho_f$ is given by $\rho_f(\varepsilon_f) = V \frac{k_f^2 \, d\Omega_{k_f} \, dk_f}{(2\pi)^3}$ , with as normalization volume V=$(2\pi)^3$. Using natural units ($\hbar = c = 1$), the incoming neutrinoflux equals $1/(2\pi)^3$. The differential cross-section is then given by

$$\frac{d^2\sigma}{d\Omega \, d\omega} = (2\pi)^4 \; k_f \varepsilon_f \sum_{s_f, s_i} \frac{1}{2J_i + 1} \sum_{M_f, M_i} \left| \left\langle f \left| \widehat{H}_W \right| i \right\rangle \right|^2 . \tag{1}$$

In the summations the initial spin states $M_i$ for the nucleus are averaged, the neutrino spins and the final nuclear states are summed. The weak interaction Hamiltonian $\widehat{H}_W$ has the current-current structure

$$\widehat{H}_W = \frac{G}{\sqrt{2}} \int d\vec{x} \;\; \hat{j}_{\mu, leptonic}(\vec{x}) \;\; \hat{J}^{\mu, hadronic}(\vec{x}) \;\; , \tag{2}$$

with G=1.16639 $10^{-11}$ $MeV^{-2}$ the weak coupling constant. The neutral leptonic current reads as

$$\begin{aligned} \hat{j}^0_\mu(x) &= \overline{\Psi}_{\nu_e}(x) \gamma_\mu (1 - \gamma_5) \Psi_{\nu_e}(x) + \overline{\Psi}_{\nu_\mu}(x) \gamma_\mu (1 - \gamma_5) \Psi_{\nu_\mu}(x) \\ &+ \overline{\Psi}_{\nu_\tau}(x) \gamma_\mu (1 - \gamma_5) \Psi_{\nu_\tau}(x) . \end{aligned} \tag{3}$$

The identical structure of the terms in equation (3) reflects the universality of the weak interactions for neutrinos of the three generations.

The weak neutral hadronic current is given by [15]

$$\begin{aligned} \widehat{J}^0_\mu &= \widehat{J}^{Vector}_\mu + \widehat{J}^{Axialvector}_\mu \\ &= \left(1 - 2\sin^2\theta_W\right) \widehat{J}^{V_3}_\mu - 2\sin^2\theta_W \, \widehat{J}^S_\mu + \widehat{J}^{A_3}_\mu \\ &= \overline{\Psi}_N \left\{ G^V_E(q^2) \gamma_\mu + \tfrac{1}{2M} G^V_M(q^2) \sigma_{\mu\nu} q^\nu + G^A(q^2) \gamma_\mu \gamma_5 \right\} . \end{aligned} \tag{4}$$

Here $\sin^2\theta_W = 0.2325$, where $\theta_W$ is the Weinberg angle. For the isospin operators, the convention $\tau_3 |p\rangle = +1$, $\tau_3 |n\rangle = -1$ is adopted. $\widehat{J}^{V_3}_\mu$ denotes the $\tau_3$ component of the electromagnetic current and $J^S_\mu$ is its scalar counterpart. The vector formfactors can be obtained directly from those in electromagnetic interactions applying the CVC theorem :

$$G^V_E = \frac{1}{2} \left(1 - 2\sin^2\theta_W\right) \tau_3 - \sin^2\theta_W , \tag{5}$$

$$G^V_M = \frac{1}{2} \left(1 - 2\sin^2\theta_W\right) (\mu_p - \mu_n) \tau_3 - \sin^2\theta_W (\mu_p + \mu_n). \tag{6}$$

$G^A$ is given by

$$G^A = - g_a \; \tau_3 = -1.262 \; \tau_3 . \tag{7}$$

In equation (4) as well as in equation (3) the $(1-\gamma_5)\,\gamma_\mu$ factor is imposed by the V-A structure of the weak interaction.

For low momentum transfers ($\kappa < 400\ \frac{MeV}{c}$), only lowest-order contributions to the hadronic current have to be retained [15] :

$$\begin{aligned}
\vec{J}_V^{\,\alpha}(\vec{x}) &= \vec{J}^{\,\alpha}_{convection}(\vec{x}) + \vec{J}^{\,\alpha}_{magnetization}(\vec{x}) \\
&\text{with} \\
&\qquad \vec{J}_c^{\,\alpha}(\vec{x}) = \frac{1}{2Mi}\sum_{i=1}^{A} G_E^{i,\alpha}\left[\delta(\vec{x}-\vec{x}_i)\overrightarrow{\bigtriangledown}_i - \overleftarrow{\bigtriangledown}_i\,\delta(\vec{x}-\vec{x}_i)\right], \\
&\qquad \vec{J}_m^{\,\alpha}(\vec{x}) = \frac{1}{2M}\sum_{i=1}^{A} G_M^{i,\alpha}\overrightarrow{\bigtriangledown}\times\vec{\sigma}_i\,\delta(\vec{x}-\vec{x}_i), \qquad (8) \\
\vec{J}_A^{\,\alpha}(\vec{x}) &= \sum_{i=1}^{A} G_A^{i,\alpha}\,\vec{\sigma}_i\,\delta(\vec{x}-\vec{x}_i), \qquad (9)
\end{aligned}$$

$$J_V^{0,\alpha}(\vec{x}) = \rho_V^{\alpha}(\vec{x}) = \sum_{i=1}^{A} G_E^{i,\alpha}\,\delta(\vec{x}-\vec{x}_i), \qquad (10)$$

$$J_A^{0,\alpha}(\vec{x}) = \rho_A^{\alpha}(\vec{x}) = \frac{1}{2Mi}\sum_{i=1}^{A} G_A^{i,\alpha}\,\vec{\sigma}_i\cdot\left[\delta(\vec{x}-\vec{x}_i)\overrightarrow{\bigtriangledown}_i - \overleftarrow{\bigtriangledown}_i\,\delta(\vec{x}-\vec{x}_i)\right]. \qquad (11)$$

Here the operator $\overrightarrow{\bigtriangledown}$ acts to the right on a ket vector, $\overleftarrow{\bigtriangledown}$ is applied to bra vectors. The summations run over all nucleons in the nucleus. The index $\alpha$ identifies the isospin character of the contribution.

Defining

$$l_\mu = \frac{1}{\sqrt{2\varepsilon_{k_f}(2\pi)^3}}\,\overline{u}^{(\nu')}(k_f,s_f)\;\gamma_\mu(1-\gamma_5)\;\frac{1}{\sqrt{2\varepsilon_{k_i}(2\pi)^3}}\,u^{(\nu)}(k_i,s_i), \qquad (12)$$

the lepton part of the transition matrixelement in the cross-section formula (1) can be written as

$$\begin{aligned}
\langle f_l\,|\hat{j}_\mu|\,i_l\rangle &= e^{-i\vec{k}_f\cdot\vec{x}}\,e^{i\vec{k}_i\cdot\vec{x}}\,l_\mu \\
&= e^{i\vec{q}\cdot\vec{x}}\,l_\mu.
\end{aligned}$$

Substituting this result and the non-relativistic limit of equations (8)-(11) in (1) and switching to a spherical basis, the cross-section formula becomes

$$\begin{aligned}
\frac{d^2\sigma}{d\Omega d\omega} = (2\pi)^4 k_f\varepsilon_f \sum_{s_f,s_i}\frac{1}{2J_i+1}\sum_{M_f,M_i}\frac{G^2}{2}\Bigg|\langle f\,|\,\Bigg\{\sum_{J=0}^{\infty}\sqrt{4\pi}\sqrt{2J+1}i^J\left[l_o\widehat{\mathcal{M}}_{J0}(\kappa)+l_3\widehat{\mathcal{L}}_{J0}(\kappa)\right] \\
+\sum_{\lambda=\pm1}\sum_{J\geq1}\sqrt{2\pi}\sqrt{2J+1}\,i^J\,l^\lambda\left[\lambda\,\widehat{\mathcal{J}}^{mag}_{J,-\lambda}(\kappa)-\widehat{\mathcal{J}}^{el}_{J,-\lambda}(\kappa)\right]\Bigg\}\,|\,i\rangle\Bigg|^2. \qquad (13)
\end{aligned}$$

Here the Rayleigh formula [16] was used to expand the exponential lepton wave-function in spherical harmonics. The multipole operators are defined as :

$$
\begin{aligned}
\widehat{\mathcal{M}}_{JM}(\kappa) &= \int d\vec{x}\, \left[ j_J(\kappa r)\, Y_J^M(\Omega_x) \right]\, \hat{J}_o(\vec{x}), \\
\widehat{\mathcal{L}}_{JM}(\kappa) &= \frac{i}{\kappa} \int d\vec{x}\, \left[ \vec{\nabla} \left( j_J(\kappa r)\, Y_J^M(\Omega_x) \right) \right] \cdot \widehat{\vec{J}}(\vec{x}), \\
\widehat{\mathcal{T}}^{el}_{JM}(\kappa) &= \frac{1}{\kappa} \int d\vec{x}\, \left[ \vec{\nabla} \times \left( j_J(\kappa r)\, \vec{\mathcal{Y}}^M_{J,J}(\Omega_x) \right) \right] \cdot \widehat{\vec{J}}(\vec{x}), \\
\widehat{\mathcal{T}}^{mag}_{JM}(\kappa) &= \int d\vec{x}\, \left[ j_J(\kappa r)\, \vec{\mathcal{Y}}^M_{J,J}(\Omega_x) \right] \cdot \widehat{\vec{J}}(\vec{x}).
\end{aligned}
\tag{14}
$$

Here, $\widehat{\mathcal{M}}_{JM}$ and $\hat{\mathcal{L}}_{JM}$ denote the Coulomb and longitudinal operator respectively, whereas $\widehat{\mathcal{T}}^{el}_{JM}$ and $\widehat{\mathcal{T}}^{mag}_{JM}$ are the transverse electric and magnetic operators. Applying the Wigner-Eckart theorem and using neutrino projection operators and trace theorems for the $\gamma$-matrices to perform the summation over the spin states, the differential cross-section for neutral-current neutrino scattering finally becomes :

$$
\left( \frac{d^2\sigma_{i\to f}}{d\Omega d\omega} \right)_{\substack{\nu \\ \bar{\nu}}} = \frac{G^2 \varepsilon_f^2}{\pi} \frac{2\cos^2\left(\frac{\theta}{2}\right)}{2J_i+1} \left[ \sum_{J=0}^{\infty} \sigma_{CL}^J + \sum_{J=1}^{\infty} \sigma_T^J \right], \tag{15}
$$

where

$$
\begin{aligned}
\sigma_{CL}^J &= \left| \left\langle J_f \left\| \widehat{\mathcal{M}}_J(\kappa) + \frac{\omega}{|\vec{q}|} \hat{\mathcal{L}}_J(\kappa) \right\| J_i \right\rangle \right|^2, \\
\sigma_T^J &= \left( -\frac{q_\mu^2}{2|\vec{q}|^2} + \tan^2\left(\frac{\theta}{2}\right) \right) \left[ \left| \left\langle J_f \left\| \widehat{\mathcal{T}}^{mag}_J(\kappa) \right\| J_i \right\rangle \right|^2 + \left| \left\langle J_f \left\| \widehat{\mathcal{T}}^{el}_J(\kappa) \right\| J_i \right\rangle \right|^2 \right] \\
&\mp \tan\left(\frac{\theta}{2}\right) \sqrt{ -\frac{q_\mu^2}{|\vec{q}|^2} + \tan^2\left(\frac{\theta}{2}\right) } \left[ 2\Re \left( \left\langle J_f \left\| \widehat{\mathcal{T}}^{mag}_J(\kappa) \right\| J_i \right\rangle \left\langle J_f \left\| \widehat{\mathcal{T}}^{el}_J(\kappa) \right\| J_i \right\rangle^* \right) \right].
\end{aligned}
$$

For each multipole transition $J^\pi$ either the vector or the axial vector part of the operators $\widehat{\mathcal{M}}_{JM}$, $\hat{\mathcal{L}}_{JM}$ and $\widehat{\mathcal{T}}^{el,mag}_{JM}$ is contributing (table I). From the expression (15) it is clear that J=0 transitions are suppressed due to the lack of a transverse contribution in these channels. Still, neutrinos are able to excite $0^-$ states in nuclei, which electrons cannot. The second and third part of the expression show that there is interference between the Coulomb and the longitudinal (CL) terms and between both transverse contributions, but not between transverse and CL terms. The only difference between neutrino and antineutrino cross-sections is in the opposite sign of the transverse interference part. From the angular dependence of the kinematic factors, it is clear that for backwards $\theta = \pi$ scattering only transverse terms contribute, while for $\theta = 0$ CL-contributions dominate.

## III. THE CONTINUUM RANDOM PHASE APPROXIMATION

The transition densities necessary to calculate the cross-section (15) are determined within a continuum random phase (CRPA) formalism [14,17–19]. In this approach, correlations between the nucleons in the nucleus are introduced. Whereas in a mean-field calculation, a nucleon experiences the presence of the others only through the mean-field they generate, the random phase approximation (RPA) additionally allows the particles to

interact by means of the residual two-body interaction. In this way, a nucleon interacting with an external field is still able to exchange energy and momentum with another particle in the nucleus. When a nucleon is excited to a particle unbound state and eventually leaves the nucleus, this must not necessarily be the one initially hit by the incoming neutrino.

The unperturbed single-particle wave-functions are generated by a Hartree-Fock calculation, using a Skyrme potential [17,21–23]. The Tamm-Dancoff (TDA) as well as the random phase approximation go one step beyond this zeroth-order mean-field approach and allow to describe a nuclear state as the coherent superposition of particle-hole contributions [30].

$$|\Psi_{TDA}\rangle = \sum_{c} \quad X_{(\Psi,C)} \quad \left|ph^{-1}\right\rangle, \tag{16}$$

$$|\Psi_{RPA}\rangle = \sum_{c} \left( X_{(\Psi,C)} \quad \left|ph^{-1}\right\rangle \; - \; Y_{(\Psi,C)} \quad \left|hp^{-1}\right\rangle \right). \tag{17}$$

The TDA accepts the shell-model closed shell configuration as the ground state, whereas excited states are described by a coherent superposition of particle-hole excitations. The random phase approximation considers particle-hole and negative energy hole-particle configurations out of a correlated ground state. The summation index C stands for all quantum numbers defining a reaction channel unambiguously : $C = \{n_h, l_h, j_h, m_h, \epsilon_h; l_p, j_p, m_p, \tau_z\}$.

The propagation of these particle-hole pairs in the nuclear medium is described by the polarization propagator. In the Lehmann representation, this particle-hole Green's function is given by [20]

$$\Pi(x_1,x_2,x_3,x_4;\omega) = \hbar \sum\!\!\!\!\!\!\int_{\hbar} \left[ \frac{\left\langle \Psi_0 \left| \hat{\psi}^\dagger(x_2)\hat{\psi}(x_1) \right| \Psi_n \right\rangle \left\langle \Psi_n \left| \hat{\psi}^\dagger(x_3)\hat{\psi}(x_4) \right| \Psi_0 \right\rangle}{\hbar\omega - (E_n - E_0) + i\eta} \right.$$
$$\left. - \frac{\left\langle \Psi_0 \left| \hat{\psi}^\dagger(x_3)\hat{\psi}(x_4) \right| \Psi_n \right\rangle \left\langle \Psi_n \left| \hat{\psi}^\dagger(x_2)\hat{\psi}(x_1) \right| \Psi_0 \right\rangle}{\hbar\omega + (E_n - E_0) - i\eta} \right], \tag{18}$$

where $|\Psi_0\rangle$ and $|\Psi_n\rangle$ denote the ground state and an excited state with eigenvalue $E_n$ of the many-particle system, respectively. The field operators $\hat{\psi}(x)$ are defined as

$$\hat{\psi}(x) = \sum\!\!\!\!\!\!\int_{\alpha} \psi_\alpha(x)\hat{c}_\alpha, \tag{19}$$

annihilating a nucleon at a point $x$. The coordinate $x$ denotes the space, spin and isospin coordinate.

In an RPA-approach, not all the degrees of freedom contained in expression (18) are considered. Only a limited class of excitations is retained. Contributions are restricted to those excitations where only one particle-one hole pairs are present, excluding the coupling to more complicated configurations of the np-nh-form.

The zeroth- and first-order approximation to the two-particle polarization propagator, respectively, read as :

$$\Pi^{(0)}(x_1,x_2,x_3,x_4;\omega) = \hbar \sum_{C} \left[ \frac{\psi_h^\dagger(x_2)\psi_p(x_1)\psi_p^\dagger(x_3)\psi_h(x_4)}{\hbar\omega - \epsilon_p + \epsilon_h + i\eta} + \frac{\psi_p^\dagger(x_2)\psi_h(x_1)\psi_h^\dagger(x_3)\psi_p(x_4)}{-\hbar\omega - \epsilon_p + \epsilon_h + i\eta} \right] \tag{20}$$

and

$$\Pi^{(1)}(x_1,x_2,x_3,x_4;\omega) = \frac{1}{\hbar}\int dx \int dx' [\ \Pi^{(0)}(x_1,x_2,x,x;\omega)\, V(x,x')\, \Pi^{(0)}(x',x',x_3,x_4;\omega) - \ \Pi^{(0)}(x_1,x_2,x',x;\omega)\, V(x,x')\, \Pi^{(0)}(x',x,x_3,x_4;\omega)], \quad (21)$$

with $V(x,x')$ the residual two-body force.

The local RPA-polarization propagator is then obtained by the iteration to all orders of this first-order contribution :

$$\Pi^{(RPA)}(x_1,x_2;\omega) = \Pi^{(RPA)}(x_1,x_1,x_2,x_2;\omega) \ = \ \Pi^{(0)}(x_1,x_2;\omega) + \frac{1}{\hbar}\int dx \int dx' \ \Pi^{(0)}(x_1,x;\omega)\, \widetilde{V}(x,x')\, \Pi^{(RPA)}(x',x_2;\omega). \quad (22)$$

Here, $\widetilde{V}$ is the antisymmetrized form of the residual interaction which in the following will be supposed to be rotationally invariant, allowing to write $\widetilde{V}(x_1,x_2)$ as

$$\widetilde{V}(x_1,x_2) = \sum_{\alpha\beta,JM} U^J_{\alpha\beta}(r_1,r_2)\ X^{JM\dagger}_\alpha(\hat{x}_1) X^{JM}_\beta(\hat{x}_2)\ , \quad (23)$$

where the $X^{JM}(\hat{x})$ represent spherical tensor operators of rank J, M.

From equations (22) and (17), it follows that the set of wave-functions, implicitly defined by

$$\begin{aligned}|\Psi_C(E)\rangle \ &= \ \left|ph^{-1}(E)\right\rangle + \int dx_1 \int dx_2 \ \ \widetilde{V}(x_1,x_2) \\ &\sum_{c'} \mathcal{P}\int d\epsilon_{p'} \left[ \frac{\psi_{h'}(x_1)\psi^\dagger_{p'}(x_1,\epsilon_{p'})}{E-\epsilon_{p'h'}} \left|p'h'^{-1}(\epsilon_{p'h'})\right\rangle \right. \\ &\left. - \frac{\psi^\dagger_{h'}(x_1)\psi_{p'}(x_1,\epsilon_{p'})}{E+\epsilon_{p'h'}} \left|h'p'^{-1}(-\epsilon_{p'h'})\right\rangle \right] \ \left\langle \Psi_0 \left|\hat{\psi}^\dagger(x_2)\hat{\psi}(x_2)\right| \Psi_C(E)\right\rangle \ , \quad (24)\end{aligned}$$

where $\mathcal{P}$ denotes the Cauchy principal value, and the $|ph^{-1}(E)\rangle$ and $|hp^{-1}(-E)\rangle$ are the unperturbed particle-hole and backward hole-particle solutions of the mean-field problem, fulfil the conditions demanded of RPA wave-functions. It can be shown that introducing the wave-functions (24) in equation (18), the resulting polarization propagator obeys the RPA Bethe-Salpeter equation (22). Furthermore, the wave-functions (24) are of the standard form (17) with

$$\begin{aligned}X_{C,C'}(E,\epsilon_{p'}) &= \delta_{C,C'}\ \delta(E-\epsilon_{p'h'}) \\ &+ \ \ \mathcal{P}\int dx_1 \int dx_2 \ \ \widetilde{V}(x_1,x_2)\ \frac{\psi_{h'}(x_1)\psi^\dagger_{p'}(x_1,\epsilon_{p'})}{E-\epsilon_{p'h'}}\ \left\langle \Psi_0 \left|\hat{\psi}^\dagger(x_2)\hat{\psi}(x_2)\right| \Psi_C(E)\right\rangle\end{aligned}$$

and

$$Y_{C,C'}(E,\epsilon_{p'}) = \qquad \int dx_1 \int dx_2 \ \ \widetilde{V}(x_1,x_2)\ \frac{\psi^\dagger_{h'}(x_1)\psi_{p'}(x_1,\epsilon_{p'})}{E+\epsilon_{p'h'}}\ \left\langle \Psi_0 \left|\hat{\psi}^\dagger(x_2)\hat{\psi}(x_2)\right| \Psi_C(E)\right\rangle \ .$$

The first term in expression (24) corresponds to the Tamm-Dancoff approximation, the second one represents the negative energy RPA contribution. From the energy dependence

of the denominators, it is clear that the first term will dominantly contribute to the total wave-function. The backward RPA contribution becomes only important for states with energies clearly distinct from those expected considering the single-particle energy levels. This makes RPA a well-suited tool for describing collective excitations in nuclei.

In angular-momentum coupled form the RPA wave-functions read as

$$|\Psi_C(JM;E)\rangle = \sum_{m_h,m_p} (-1)^{j_h-m_h} \langle j_h \ -m_h \ j_p \, m_p | J \, M\rangle \ |\Psi_C(E)\rangle \,, \tag{25}$$

where C now denotes a reaction channel in the coupled scheme : $C = \{n_h, l_h, j_h, m_h, \epsilon_h; l_p, j_p, m_p, \tau_z\}_{JM}$. From the wave-functions (25) the correctly normalized solutions of the scattering problem can be obtained by taking suitable linear combinations. Defining the K-matrix by

$$K^J_{C,C'} = \frac{-1}{2J+1} \sum_{\alpha,\beta} \int dr_1 \int dr_2 \ U^J_{\alpha\beta}(r_1,r_2) \ \left\langle h' \left|\left| X^J_\alpha(x_1) \right|\right| p'(E+\epsilon_{h'}) \right\rangle^*_{r_1} \left\langle \Psi_0 \left|\left| X^J_\beta(x_2) \right|\right| \Psi_C(J;E) \right\rangle_{r_2} , \tag{26}$$

where the r-subscript of the transition densities denotes that all coordinates except the radial one have been integrated, it can be shown that the wave-functions constructed by putting

$$\left|\Psi^+_C(JM;E)\right\rangle = \sum_{C'_{open} \,:\, \epsilon_p = \epsilon_h + E > 0} \left[1 + i\pi K^J\right]^{-1}_{C,C'} \ |\Psi_{C'}(JM;E)\rangle \,, \tag{27}$$

contain asymptotically only one incoming wave. They allow to describe systems where one particle is excited to an unbound state with $\epsilon_p > 0$, and is able to escape from the nuclear potential. Furthermore they obey the same normalization conditions as the unperturbed $|ph^{-1}\rangle$ wave-functions. From the above, if follows that the wave-functions (27) are the ones needed to evaluate the transition densities in the cross-section (15).

Defining the unperturbed radial response functions as

$$\int dr \int dr' \ R^{(0)}_{\eta\mu;JM}(r,r';E) = \frac{1}{\hbar} \int dx \int dx' \ \ X_{\eta JM}(x) \ \Pi^{(0)}(x,x';\omega) \ X^\dagger_{\eta' JM}(x') \,, \tag{28}$$

the RPA transition densities are determined by the set of coupled integral equations

$$\begin{aligned} \left\langle \Psi_0 || X_{\eta J} || \Psi_C(J;E) \right\rangle_r &= - \left\langle h || X_{\eta J} || p(\epsilon_{ph}) \right\rangle_r \\ &+ \sum_{\mu,\nu} \int dr_1 \int dr_2 \ U^J_{\mu\nu}(r_1,r_2) \ \Re \left( R^{(0)}_{\eta\mu;J}(r,r_1;E) \right) \ \left\langle \Psi_0 || X_{\nu J} || \Psi_C(J;E) \right\rangle_{r_2} . \end{aligned} \tag{29}$$

Discretizing these equations on a mesh in the radial coordinate, the transitions densities for each reaction channel (29) are obtained as the solutions of the matrix equation

$$\rho^{RPA}_C \ = \ - \frac{1}{1 - R\,U} \ \rho^{HF}_C . \tag{30}$$

Here $\rho^{RPA}$ and $\rho^{HF}$ represent column vectors containing the RPA and the Hartree-Fock transition densities for all included interaction channels $\eta$ and for a number of mesh points in coordinate space. $R$ and $U$ are block matrices containing the unperturbed response function

(28) and the radial part of the interaction (23), evaluated at the appropriate channels and r-values. The discretization in coordinate-space is well under control. It does not demand large numbers of mesh-points for the calculated transition densities to become mesh independent, thus keeping the dimension of matrix inversions to be performed, sufficiently small. From the form of equation (30) it is clear that the wave-functions (24) can be considered as the solution to the RPA equivalent of the Lippmann-Schwinger integral scattering equations. In equation (30) as well as in equation (29), the minus sign arises from the phase convention adopted in the definition of the K-matrix (26).

This formalism has the interesting feature that the unperturbed polarization operator (20) can be written as

$$\Pi^{(0)}(x_1,x_2,x_3,x_4;\omega) = \hbar \sum_h \Big\{ \psi_h^\dagger(x_2) g(x_1,x_3;E+\epsilon_h)\psi_h(x_4)$$

$$+ \psi_h(x_1) g(x_4,x_2;-E+\epsilon_h)\psi_h^\dagger(x_3) + \; 2\pi i \sum_{h'} \psi_h^\dagger(x_2)\psi_{h'}^\dagger(x_3)\psi_h(x_4)\,\delta(E+(\epsilon_h-\epsilon'_h)\Big\}, \quad (31)$$

in which g denotes the single-particle Green's function

$$g(x,x';E) \; = \sum\!\!\!\!\!\!\int_\alpha \; \psi_\alpha(x)\,\frac{1}{E-\epsilon_\alpha+i\eta}\,\psi_\alpha^\dagger(x'). \quad (32)$$

It is possible to determine this quantity exactly, without performing the infinite sum over all eigenstates $\alpha$ of the single-particle Hamiltonian. Furthermore the summation in (31) is only over a limited number of hole states. Thus, treating the RPA-equations in coordinate space allows to deal with the energy continuum in an exact way, without cut-off nor discretization of the excitation energies.

## IV. THE SKE2 INTERACTION

The Hartree-Fock and RPA calculations were performed with an extended Skyrme force. The parameter values used to obtain the presented results are those of the SkE2-parametrization [17,21–23]. This parameter set was designed to yield a realistic description of nuclear structure properties in both the particle-particle (pairing properties) and in the particle-hole channels and this over the whole mass table. This is done by replacing only part of the three-particle contribution by a momentum dependent two-particle term. The extra free parameter thus obtained is used to guarantee correct two-body characteristics in nuclei containing few valence nucleons outside of the closed shells.

In coordinate space , the antisymmetrized residual interaction takes the form

$$\begin{aligned} V(\vec{r}_1,\vec{r}_2) = {} & t_0\,(1+x_0\hat{P}_\sigma)\,\delta(\vec{r}_1-\vec{r}_2) \\ & - \frac{1}{8}t_1\left[\left(\overleftarrow{\nabla}_1-\overleftarrow{\nabla}_2\right)^2\delta(\vec{r}_1-\vec{r}_2)+\delta(\vec{r}_1-\vec{r}_2)\left(\overrightarrow{\nabla}_1-\overrightarrow{\nabla}_2\right)^2\right] \\ & + \frac{1}{4}t_2\left(\overleftarrow{\nabla}_1-\overleftarrow{\nabla}_2\right)\delta(\vec{r}_1-\vec{r}_2)\left(\overrightarrow{\nabla}_1-\overrightarrow{\nabla}_2\right) + \frac{e^2}{|\vec{r}_1-\vec{r}_2|} \\ & + i\,W_0\,(\vec{\sigma}_1+\vec{\sigma}_2)\cdot\left(\overleftarrow{\nabla}_1-\overleftarrow{\nabla}_2\right)\times\delta(\vec{r}_1-\vec{r}_2)\left(\overrightarrow{\nabla}_1-\overrightarrow{\nabla}_2\right) \end{aligned}$$

$$+\frac{1}{6}\,t_3\,(1-x_3)\,(1+\hat{P}_\sigma)\,\rho\left(\frac{\vec{r}_1+\vec{r}_2}{2}\right)\,\delta(\vec{r}_1-\vec{r}_2)+x_3\,t_3\,\delta(\vec{r}_1-\vec{r}_2)\delta(\vec{r}_1-\vec{r}_3)$$
$$-\frac{1}{24}\,t_4\,\left\{\left[\left(\overleftarrow{\bigtriangledown}_1-\overleftarrow{\bigtriangledown}_2\right)^2+\left(\overleftarrow{\bigtriangledown}_2-\overleftarrow{\bigtriangledown}_3\right)^2+\left(\overleftarrow{\bigtriangledown}_3-\overleftarrow{\bigtriangledown}_1\right)^2\right]\,\delta(\vec{r}_1-\vec{r}_2)\delta(\vec{r}_1-\vec{r}_3)\right.$$
$$\left.+\,\delta(\vec{r}_1-\vec{r}_2)\delta(\vec{r}_1-\vec{r}_3)\,\left[\left(\overrightarrow{\bigtriangledown}_1-\overrightarrow{\bigtriangledown}_2\right)^2+\left(\overrightarrow{\bigtriangledown}_2-\overrightarrow{\bigtriangledown}_3\right)^2+\left(\overrightarrow{\bigtriangledown}_3-\overrightarrow{\bigtriangledown}_1\right)^2\right]\right\}, \quad (33)$$

with $P_\sigma$ the spin exchange operator. Table II illustrates the parameter values for the SkE2-set.

In the calculation of the transition densities, only the most important channels resulting from (33) are taken into account in the equations (23). For natural parity calculations these are :

$$Y_J,\ [Y_J\otimes\vec{\sigma}]_J\,,\ \left[Y_{J\pm1}\otimes(\overrightarrow{\bigtriangledown}\pm\overleftarrow{\bigtriangledown})\right]_J,\ \left[Y_J\otimes(\overrightarrow{\bigtriangledown}^2+\overleftarrow{\bigtriangledown}^2)\right]_J. \quad (34)$$

For unnatural parity transitions, the dominant channels are

$$[Y_{J\pm1}\otimes\vec{\sigma}]_J\,,\ \left[Y_J\otimes(\overrightarrow{\bigtriangledown}\pm\overleftarrow{\bigtriangledown})\right]_J,\ \left[[Y_J\otimes(\overrightarrow{\bigtriangledown}-\overleftarrow{\bigtriangledown})]_J\otimes\vec{\sigma}\right]_J,$$
$$\left[\left[Y_J\otimes(\overrightarrow{\bigtriangledown}-\overleftarrow{\bigtriangledown})\right]_{J\pm1}\otimes\vec{\sigma}\right]_J \text{ and } \left[[Y_{J\pm1}\otimes(\overrightarrow{\bigtriangledown}^2-\overleftarrow{\bigtriangledown}^2)]_J\otimes\vec{\sigma}\right]_J, \quad (35)$$

where all operators can be combined with the isospinoperators 1 and $\vec{\tau}$. These contribute in a coherent way in the RPA-equations (29) and (30).
As the same interaction with the same parameter values is adopted for the calculation of the unperturbed as well as the RPA wave-functions, the formalism is self-consistent with respect to the residual interaction used.

## V. APPLICATIONS TO $^{16}$O AND $^{12}$C.

### A. The Nucleus $^{16}$O

As one of the major products of the thermonuclear burning processes in massive stars, $^{16}$O plays an important role in explosive nucleosynthesis. Moreover, having closed proton and neutron shells, the lack of major nuclear structure difficulties, makes it a good test for the reliability of the formalism. Therefore, the study of neutrino-nucleus interactions with the CRPA formalism was started with cross-section calculations for the neutral-current reaction

$$^{16}O\ +\ \nu\ \rightarrow\ ^{16}O^*\ +\ \nu'.$$

In all of the following results, calculations were performed with an incoming neutrino energy $\epsilon_i$=50 MeV. Multipoles up to J=4 were taken into account. Contributions of higher-order multipole excitations were found to be negligibly small. The differential neutrino scattering cross-sections are of the order of $10^{-42}$ cm$^2$ per MeV. In figure 1, we show the

total cross-section and its dominant multipole contributions. At excitation energies between 20 and 25 MeV, the broad resonance structure of the giant dipole resonance shows up. At energies below 20 MeV, smaller peaks, related to excitations with a stronger single-particle character, are present. In RPA results, resonances are pushed to somewhat higher energies than those in mean-field calculations due to the repulsive character of the residual interaction in the isovector channels. For excitation energies above $\sim$ 30 MeV, the cross-section decreases almost purely exponentially, according to the energy dependence of equation (15). The J=1 excitations are clearly prominent. In figure 2 we show some less important multipole contributions. J=0 excitations are suppressed due to the fact that only Coulomb and longitudinal terms contribute to these channels. But still, some clear $0^-$ resonances show up in the differential cross-sections.

In figure 3, we carry out a comparison between the contribution of the axial and the axial vector part of the hadronic current to the total cross-section. The axial vector current is clearly more sensitive to the weak neutrino probes. The vector contribution is suppressed by almost two orders of magnitude. The splitting of the cross-section in a vector and an axial vector part excludes the interference contribution. This explains the discrepancy between the sum of both curves in figure 3 and the total cross-section.

Due to the fact that the axial vector current is completely isovector, isovector excitations will dominate isoscalar ones, as figure 4 indeed illustrates. The reason for the large suppression of the isoscalar excitions is twofold : not only is the axial vector current not contributing to isoscalar transitions, but due to the $\sin^2\theta_W$-factor the isoscalar form factors are considerably smaller than the vector ones as well.

In figure 5 we then compare the contribution of the different operators (14) to the cross-section. Transverse transitions are clearly prominent. The difference between the sum of transverse and CL-terms and the total cross-section is again due to the transverse interference term. According to equation (15) it is this interference contribution that is responsible for the difference in the nuclear response to neutrino and antineutrino perturbations. The sign of the interference term determines which cross-section will be dominant. In figure 6 we show that generally neutrino cross-sections are slightly larger than antineutrino cross-sections. Only round 23 MeV, the interference term changes sign and antineutrino excitations become more important.

All these results were obtained with the SkE2-Skyrme force. To investigate the sensitivity of our calculations to the choice of the interaction, we repeated our calcultions using a Landau-Migdal residual two-body force. The Landau-Migdal parameters were taken from reference [24]. In figure 7 we show that, apart from slight differences in the relative weight of the resonances, the cross-sections obtained using different residual interactions are in good agreement.

Our self-consistent calculations substantiate the results of Kolbe et al [5,6] on neutral-current reactions. Contrary to the present work, there the CRPA-equations are solved using the techniques proposed by [25]. The standard RPA-equations (17) are extended to the continuum by the introduction of an integration over the excitation energies. The resulting integro-differential equations are then solved by an expansion in Weinberg states, already having the correct asymptotic behaviour and thus making a fast convergence possible. As residual interaction an effective force derived from the Bonn meson exchange potential is used. The single-particle wave-functions are generated using a Woods-Saxon potential. A

comparison of results obtained with the different methods makes clear that total cross-sections as well as cross-section for transitions to specific $J^\pi$ final states show remarkable agreement in overall strength and in the position of the resonances. Moreover, also the more detailed conclusions concerning relative strength of vector and axial vector, neutrino and antineutrino, isovector and isoscalar, and transverse and Coulomb-longitudinal contributions are in excellent agreement.

### B. The Nucleus $^{12}$C

As $^{12}$C is known to be deformed in its ground state, whereas the Hartree-Fock calculation assumes the nucleus to have a spherical ground state, the single-particle wave-functions for $^{12}$C were determined in a different way : the unperturbed wave-functions were generated with a Woods-Saxon potential, yielding a more reliable splitting between the single-particle energy levels. The Woods-Saxon parameters were taken from reference [26]. Thereby, the full self-consistency is spoiled but it is clearly an approach that allows to take into account some effects of the deformed ground state, albeit in a phenomenological way.

Cross-sections for neutral-current neutrino scattering on $^{12}$C show mainly the same behaviour as those for the reaction $^{16}O(\nu,\nu')^{16}O^*$. In figure 8 we show the differential cross-section and the principal multipole contributions $J^\pi=1^+$, $1^-$ and $2^-$. Again axial vector and isovector excitations are prominent. Coulomb and longitudinal contributions are suppressed. Neutrino cross-sections dominate antineutrino excitations. As was the case for $^{16}$O, our results are in good agreement with those of Kolbe et al [5,6].

## VI. NEUTRINO NUCLEOSYNTHESIS

As neutrinos only participate in weak interaction processes and cross-sections for scattering reactions involving neutrinos are very small, the importance of neutrinos to astrophysical processes has long been underestimated. However, models describing the explosion mechanism of type II supernovae provide an important role for neutrinos in these processes [1,2].

When, at the end of the lifetime of a massive star, its thermonuclear fuel is exhausted, the core of the star contracts. The lack of elements left to burn and produce the pressure needed to remain in hydrostatic equilibrium, makes it impossible for the star to prevent the implosion of its own core. The neutronization processes taking place in the imploding starcore produce large amounts of neutrinos. The densities are that high that despite their small interaction cross-sections, the neutrinos are trapped and forced to join the infalling material of the collapsing star core. When nuclear densities are reached in the centre of the imploding star, the core bounces. The movement of the infalling material is reversed, temperature and density drop. The trapped neutrinos are released and the cooling of the new neutron star by the production and subsequent emission of neutrino pairs starts. This causes a flux of $\sim 10^{58}$ neutrinos, representing an energy of $10^{53}$ erg, approximately 99% of the total released gravitational energy. Although the neutrinos are only weakly interacting, this enormous amount of particles and energy travelling through the different layers of the star is able to cause a considerable transformation of the elements synthesized during the preceding thermonuclear burning processes in the life of the star.

The energy distribution of the supernova neutrinos is described by a Fermi-Dirac spectrum [1]:

$$n_\nu(E,T) = \frac{N}{T^3}\,\frac{E^2}{1+e^{E/T}}, \tag{36}$$

where the normalization factor N equals 0.533. The temperature of the spectra amounts approximately 3.5 MeV for electron neutrinos and 5 MeV for electron antineutrinos [27]. This temperature difference arises from the larger amount of neutrons in the core of a star which favors the reaction

$$n \,+\, \nu_e \;\rightarrow\; p \,+\, e^-. \tag{37}$$

Neutrinos participate in more reactions than antineutrinos and thus experience more difficulties to leave the star. Their trapping radius is larger than the one for antineutrinos. As a consequence, neutrinos escape from a region further away from the centre of the star, where the temperature is lower. In a similar way, $\mu$- and $\tau$-neutrinos have spectra with higher temperatures. As typical supernova energies are not high enough to produce heavy leptons, heavy flavor neutrinos do not participate in charged current reactions. They escape from regions closer to the starcentre with temperatures of 8-10 MeV. As the cross-sections are roughly proportional to the square of the incoming neutrino energy, the higher temperature $\mu$- and $\tau$-neutrinos and neutral-current reactions will dominate nucleosynthesis processes.

In figure 9 we show the results for calculations where the $^{16}$O cross-sections have been folded with a Fermi-Dirac spectrum with temperatures between 4 and 12 MeV. Table VIII summarizes the total cross-sections for the Hartree-Fock and the CRPA calculation. The results obtained in the present study are in good agreement with those of references [5] and [1] and thus substantiate the reliability (cross-section magnitude and overall shape) of CRPA calculations determining neutrino-nucleus scattering processes.

The sensitivity of the cross-sections to the temperature is due to the strong energy dependence of the nuclear response in the considered energy region. The temperatures studied correspond to average neutrino energies between 12 and 38 MeV. The large differences are then easily explained by noting that the continuum in $^{16}$O only opens at $\sim$11 MeV. Next to a bare energy effect, the number of particles with energies above the $^{16}$O particle threshold increases considerably with the temperature of the neutrino distribution, enhancing the cross-sections accordingly. As a consequence, it is mainly the neutrinos in the high-energy tail of the spectrum that are responsible for the excitation of nuclei. It is therefore important to have a good description of this part of the energy spectrum for supernova neutrinos. Monte-Carlo simulations of neutrino transport in supernovae indicate that in this energy region, the spectrum is somewhat depleted compared to the distribution (36). The tail of the Fermi-Dirac distribution can be adjusted to a more accurate reproduction of the actual supernova spectrum by bringing in a chemical potential [28,29] . The new neutrino energy spectrum then reads as

$$n_\nu(E,T,\alpha) = \frac{N_\alpha}{T^3}\,\frac{E^2}{1+e^{(E/T+\alpha)}}, \tag{38}$$

where $\alpha$ is the parameter associated with the non-zero chemical potential and $N_\alpha$ is a normalization factor depending on $\alpha$. In figure 10 we show how the introduction of a non-zero

$\alpha$-parameter affects the differential cross-sections. The influence of such an adjustment on the total cross-sections is relatively small. Only in the giant dipole resonance region the adjustment of the neutrino spectrum causes slight changes in the results. Further investigations showed that differences caused by the variation of the parameter $\alpha$ in the range $\alpha$=3 to $\alpha$=6 have a negligible influence on the results.

In figure 11 and table IV we show a similar picture for neutrino nucleosynthesis reactions on $^{12}$C. Here, similar conclusions as in the case of $^{16}$O can be drawn in comparison with other calculations.

## VII. ON THE RELIABILITY OF THE TDA AND RPA CALCULATIONS

Starting from the CRPA calculations, as discussed in sections 5 and 6, one can easily compare with the results from TDA calculations by just switching off the backward-going term in the wave functions (see expression (24)). Due to the energy factors appearing in the denominators of equation (24), the latter terms are not expected to have a major influence on the resulting transition densities. Nevertheless, the comparison in figure 12, of the TDA and RPA results, shows some important differences. The contribution of $1^+$, $2^-$ and $0^+$ excitations are unproportionally large in TDA, compared to those in RPA.

Moreover, the TDA solutions are unstable against small changes in the residual interaction. This can easily be illustrated by using different two-body forces. In figure 13 we compare the RPA and TDA results using the SkE2-Skyrme and Landau-Migdal forces. The Landau-Migdal parameters were taken from reference [24]. Whereas RPA results obtained using different forces ressemble each other rather well, the outcome of the TDA calculations is extremely sensitive to the force used, as is illustrated in figure 13.

The anomalous behaviour of the TDA solution may well be caused by the intrinsic asymmetry underlying the TDA equations [30]. Whereas in the RPA formalism the groundstate is allowed to contain correlations, and is thus treated on an equal basis with all excited states, the TDA groundstate is a static reference state. The lack of backward going terms in the TDA equations implies the use of a closed-shell state as the TDA vacuum.

Furthermore it should be stressed that even the RPA results have to be considered with extreme care, especially for excitation energies below $\sim$25 MeV. The large contributions introduced by the RPA correlations compared to the Hartree-Fock results, as is illustrated in figure 14, make it difficult to see the RPA as a correction that can be handled within perturbation theory. These differences are indications that more complex nuclear configurations should be incorporated in order to give a more reliable description of both the resonance energies and widths in the giant resonance region. A related problem is the sensitivity of the results to the choice of single-particle energies and wave-functions, which makes it hard to obtain unambiguous cross-section results.

## VIII. CONCLUSION

In the present paper, we have carried out RPA studies of neutrino-nucleus scattering reactions and corresponding nucleosynthesis processes. The RPA equations have been studied

using a Green's function approach with an effective Skyrme force (SkE2) and a Landau-Migdal force as residual two-body interactions. The SkE2-force already showed its strength in evaluating various electromagnetic processes. We now have extended applications into the weak interaction sector.

Besides performing detailed calculations for $^{16}$O and $^{12}$C, we have carefully studied the consequences of using TDA instead of RPA, and the effects of using different residual interactions in order to obtain conclusions on the reliability of present-days RPA calculations.

A first important conclusion is that our results substantiate earlier ones, obtained by Kolbe et al [5,6] using a different technique to solve the RPA equations. Moreover, the RPA-results do not seem to be very sensitive to the particular choice of the residual two-body force. We also noted that the TDA results differ substantially from RPA results and thus much caution has to be taken when using the former method. As expected there also appears a clear sensitivity to the use of the particular unperturbed single-particle energy spectrum used as input. This can cause shifts in the resonance structure. These latter conclusions also point towards the need to incorporate more complex configurations in order to produce both the correct excitation energies and widths of the various resonances.

In $^{16}$O as well as in $^{12}$C the dominant multipole transitions are $J^\pi = 1^-, 1^+, 2^-$. The $J = 0$ exitations are suppressed. Due to the dominance of the axial vector contribution, isovector excitations are clearly prominent. In both nuclei, neutrino cross-sections are slightly larger than cross-sections for excitations induced by antineutrinos.

Both nuclei studied play an important role in explosive nucleosynthesis. We made an estimate of the importance of the reactions studied to neutrino nucleosynthesis by folding the neutrino-nucleus scattering cross-sections with a Fermi-Dirac energy spectrum. The resulting cross-sections depend sensitively on the temperature of the neutrino spectrum. The influence of the introduction of a chemical potential is rather small.

**Acknowledgment.** One of the authors (NJ) thanks the University Research Board (BOZF), SR, KH and JR are grateful to the Fund for Scientific Research (FWO) Flanders for financial support. Moreover, KH thanks CERN for financial support in the later stages of this work. The authors are grateful to M. Arnould, S. Gloriely, E. Kolbe, K. Langanke and F. Thieleman for many fruitful discussions.

# REFERENCES


[1] S.E. Woosley, D.H. Hartmann, R.D. Hofman and W.C. Haxton, ApJ 356, 272 (1990).
[2] W.C. Haxton, Nucl. Phys. A553, 397c (1993).
[3] W.M. Alberico, M.B. Barbaro, S.M. Bilenky, J.A. Caballero, C. Giunti, C. Maieron, E. Moya de Guerra and J.M. Udías, Nucl. Phys. A623, 471 (1997).
[4] H. Kim, J. Piekarewicz, C.J. Horowitz, Phys. Rev. C 51, 2739 (1994).
[5] E. Kolbe, K. Langanke, S. Krewald and F.K. Thielemann, Nucl. Phys. A540, 599 (1992).
[6] E. Kolbe *Untersuchungen zur inelastischen Neutrinostreuung an Kernen und Anwendungen in der Kern- und Astrophysik*, Phd-thesis, Westfälischen Wilhelms-Universität Münster (1992).
[7] N. Auerbach, N. Van Giai and O.K. Vorov, Phys. Rev. C 56, 2368 (1997).
[8] S.K. Singh, Nimai C. Mukhopadhyay and E. Oset, Phys. Rev. C 57, 2687 (1998).
[9] C. Athanassopoulos *et al.*, Phys. Rev. C 56, 2806 (1997).
[10] B. Zeitnitz, Prog. Part. Nucl. Phys. 32, 351 (1994).
[11] E. Kolbe, K. Langanke, F.K. Thielemann and P. Vogel Phys. Rev. C 52, 3437 (1995).
[12] E.Kolbe, Phys. Rev. C 54, 1741 (1996).
[13] E. Kolbe, K. Langanke and P. Vogel, Nucl. Phys. A613, 382 (1997).
[14] J. Ryckebusch, M. Waroquier, K. Heyde, J. Moreau and D. Ryckbosch, Nucl. Phys. A476, 273 (1988).
[15] J.D. Walecka *Semileptonic Weak Interactions in Nuclei* in *Muon Physics II - Weak Interactions* edited by V.W. Hughes and C.S. Wu (Academic Press, New York 1975).
[16] G. Arfken *Mathematical Methods for Physicists, Third Edition* (Academic Press, 1985).
[17] J. Ryckebusch, K. Heyde, D. Van Neck and M. Waroquier, Nucl. Phys. A503, 694 (1989).
[18] G.F. Bertsch an S.F. Tsai, Phys. Rept. 18 C, 125 (1975).
[19] S.F. Tsai, Phys. Rev. C 17, 1862 (1978).
[20] A.L. Fetter and J.D. Walecka *Quantum Theory of Many-Particle Systems* (McGraw-Hill Book Company, New York 1971).
[21] M. Waroquier, J. Sau, K. Heyde, P. Van Isacker and H. Vinckx, Phys. Rev. C 19, 1983 (1979).
[22] M. Waroquier, K. Heyde and G. Wenes, Nucl. Phys. A404, 269 (1989).
[23] M. Waroquier, J. Ryckebusch, J. Moreau, K.Heyde, N. Blasi, S.Y. van de Werf and G. Wenes, Phys. Rept. 148, 249 (1987).
[24] G. Co' and S. Krewald, Nucl. Phys. A433, 392 (1985).
[25] M. Buballa, S. Drożdź, S. Krewald and J. Speth, Ann. of Phys. 208, 364 (1991).
[26] G. Co' and S. Krewald, Phys. Lett. 137 B, 145 (1984).
[27] K. Langanke, Nucl. Phys. A621, 351c (1997).
[28] H.-T. Janka and W. Hillebrandt A&AS 78, 373 (1989).
[29] H.-T. Janka and W. Hillebrandt A&A 224, 49 (1989).
[30] D.J. Rowe *Nuclear Collective Motion* (Methuen and Co, London 1970).

## TABLES

| | $\mathcal{M}_J$ | $\mathcal{L}_J$ | $\mathcal{T}_J^{el}$ | $\mathcal{T}_J^{mag}$ |
|---|---|---|---|---|
| natural parity $(l_p + l_h + J = even)$ | V | V | V | A |
| unnatural parity $(l_p + l_h + J = odd)$ | A | A | A | V |

TABLE I. Parity of vector and axial vector part of the different multipole operators.

| $t_0$ | $t_1$ | $t_2$ | $t_3$ | $t_4$ | $x_0$ | $W_0$ | $x_3$ |
|---|---|---|---|---|---|---|---|
| -1299.30 | 802.41 | -67.89 | 19558.96 | -15808.79 | 0.270 | 120 | 0.43 |
| $MeV\ fm^3$ | $MeV\ fm^5$ | $MeV\ fm^5$ | $MeV\ fm^6$ | $MeV\ fm^8$ | | $MeV\ fm^5$ | |

TABLE II. Parameter set for the SkE2-interaction.

| T (MeV) | | | 4 | 6 | 8 | 10 | 12 |
|---|---|---|---|---|---|---|---|
| $^{16}O$ | $\frac{d\sigma}{d\omega}$ $(10^{-42}\ cm^2)$ | MF | 0.0033 | 0.045 | 0.22 | 0.71 | 1.7 |
| | | CRPA | 0.0056 | 0.070 | 0.32 | 1.0 | 2.2 |

TABLE III. Cross-section per nucleon for the reaction $^{16}O + \nu_{FD} \rightarrow ^{16} O^* + \nu'$, averaged over neutrinos and antineutrinos and over a Fermi-Dirac distribution with temperature T.

| T (MeV) | | | 4 | 6 | 8 | 10 | 12 |
|---|---|---|---|---|---|---|---|
| $^{12}C$ | $\frac{d\sigma}{d\omega}$ $(10^{-42}\ cm^2)$ | MF | 0.0018 | 0.024 | 0.12 | 0.41 | 1.0 |
| | | CRPA | 0.0016 | 0.026 | 0.14 | 0.45 | 1.1 |

TABLE IV. Cross-section per nucleon for the reaction $^{12}C + \nu_{FD} \rightarrow ^{12} C^* + \nu'$, averaged over neutrinos and antineutrinos and over a Fermi-Dirac distribution with temperature T.

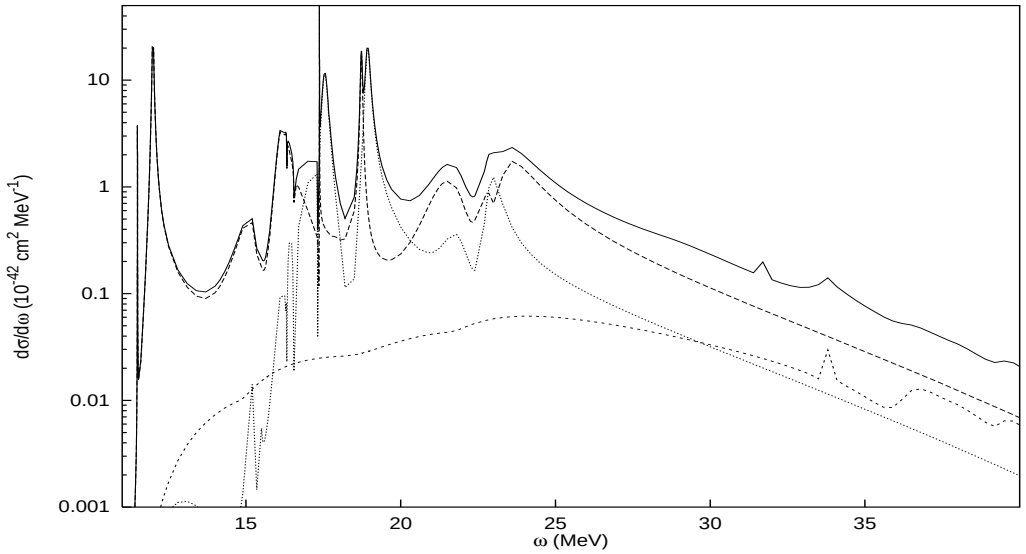


FIG. 1. Cross-section for the reaction $^{16}O + \nu_{50\,MeV} \rightarrow {}^{16}O^* + \nu'$ (full line) and its dominant multipole contributions. $J^\pi = 1^-$ (dashed line), $J^\pi = 1^+$ (small dashes below) and $J^\pi = 2^-$ (dotted line). The total cross-section includes multipoles up to J=4.

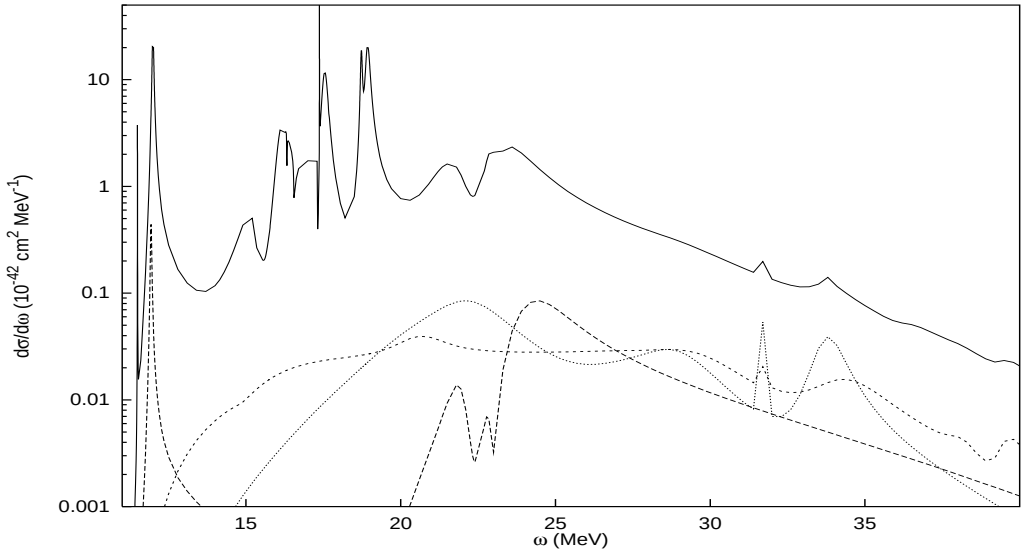


FIG. 2. Cross-section for the reaction $^{16}O + \nu_{50\,MeV} \rightarrow {}^{16}O^* + \nu'$ (full line) and some more reluctant multipole contributions. $J^\pi = 0^-$ (dashed line), $J^\pi = 2^+$ (short-dashed) and $J^\pi = 3^+$ (dotted line).

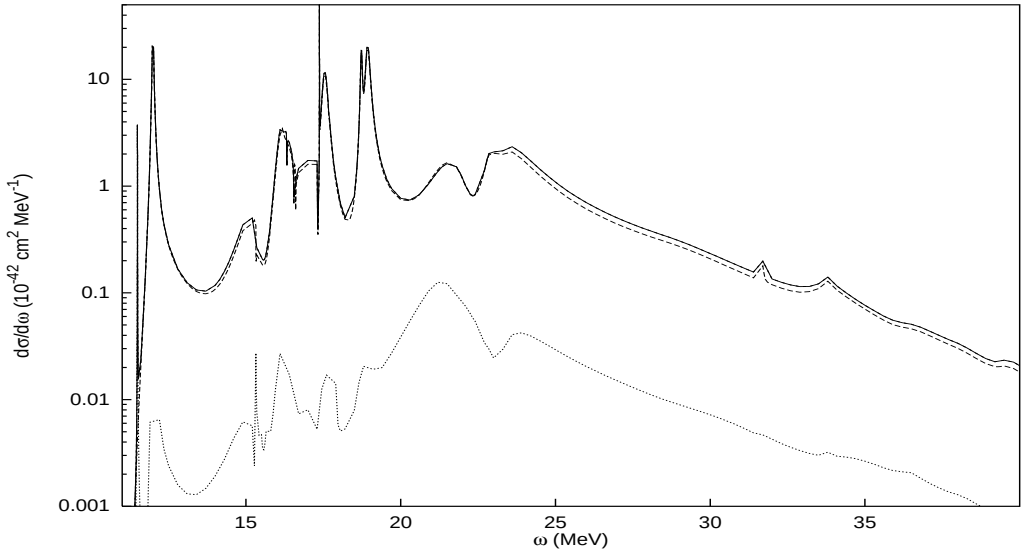


FIG. 3. Comparison between the vector (dotted) and the axial vector (dashed line) contribution to the reaction $^{16}O(\nu,\nu')^{16}O^*$.

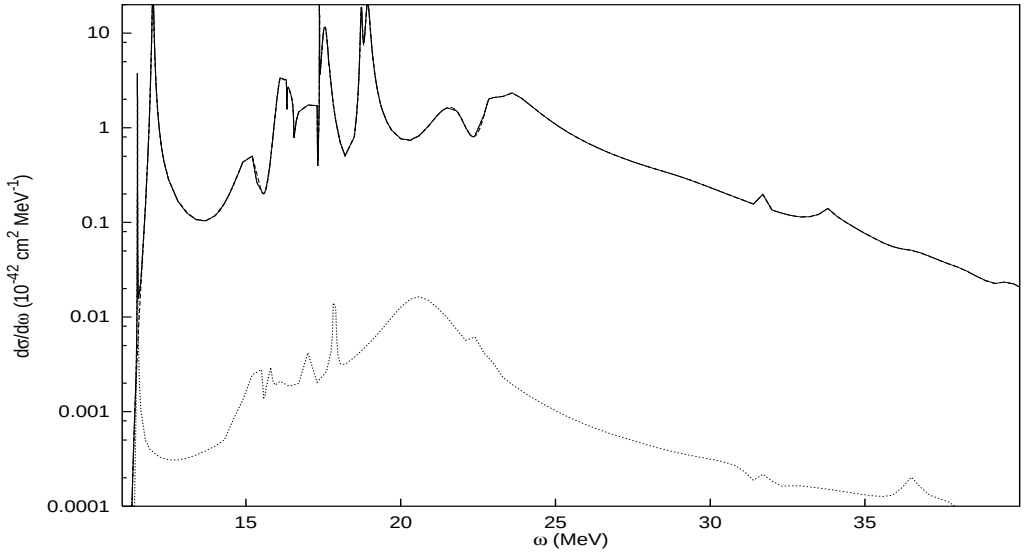


FIG. 4. Comparison between the isovector (dashed line) and the isoscalar (dotted) contribution to the reaction $^{16}O(\nu,\nu')^{16}O^*$. The isovector curve almost coincides with the total cross-section.

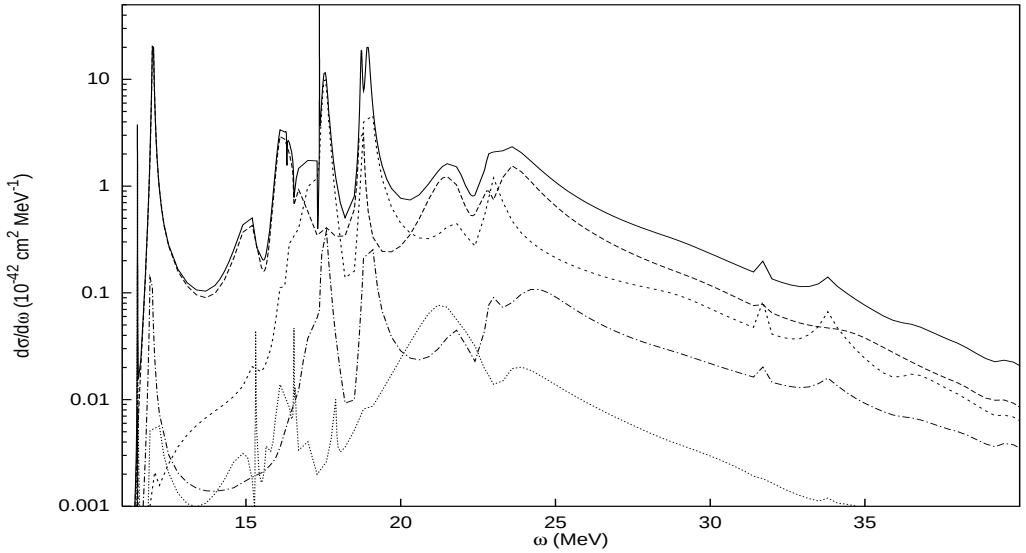


FIG. 5. Coulomb (dotted line), longitudinal (dashed-dotted), transverse electric (shortdashed) and transverse magnetic (dashed) contributions to the reaction $^{16}O(\nu,\nu')^{16}O^*$. The full line gives the total differential cross-section.

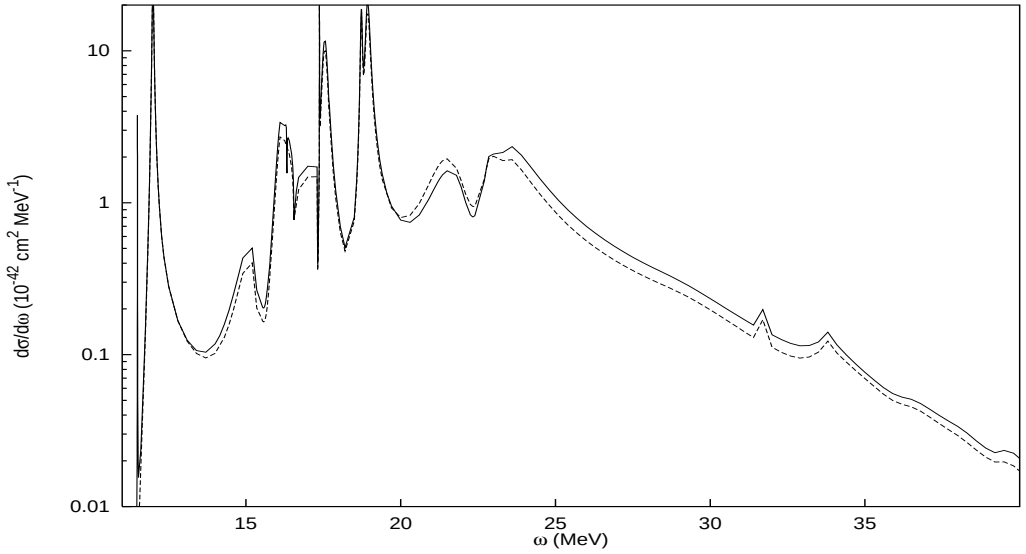


FIG. 6. Cross-section for the reactions $^{16}O + \nu_{50MeV} \rightarrow {}^{16}O^* + \nu'$ (full line) and $^{16}O + \overline{\nu}_{50MeV} \rightarrow {}^{16}O^* + \overline{\nu}'$ (dashed line).

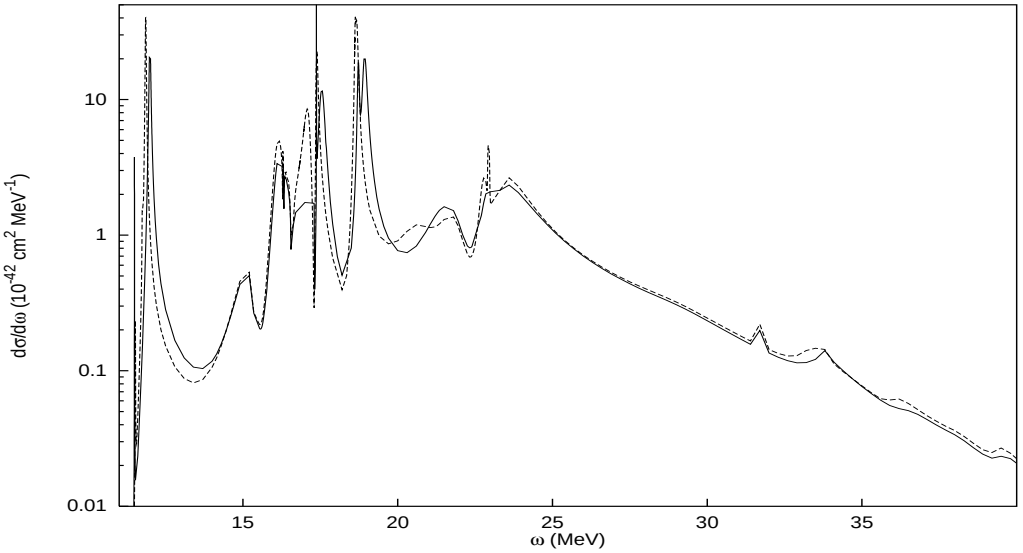


FIG. 7. Comparison of RPA results obtained with the Skyrme (full line) and Landau-Migdal (dashed) residual two-body interaction. The incoming neutrino energy is 50 MeV. All multipoles up to J=4 are taken into account.

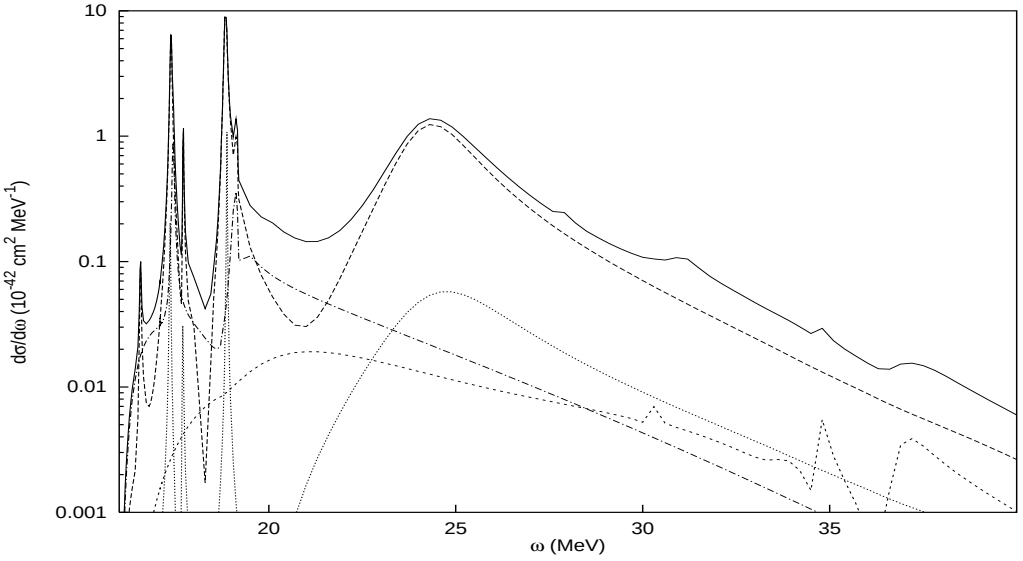


FIG. 8. Cross-section for the reaction $^{12}C + \nu_{50\,MeV} \rightarrow {}^{12}C^* + \nu'$ (full line) and its dominant multipole contributions. $J^\pi = 1^-$ (dashed line), $J^\pi = 1^+$ (small dashes below), $J^\pi = 0^-$ (dotted line) and $J^\pi = 2^-$ (dashed-dotted). The total cross-section includes multipoles up to J=4.

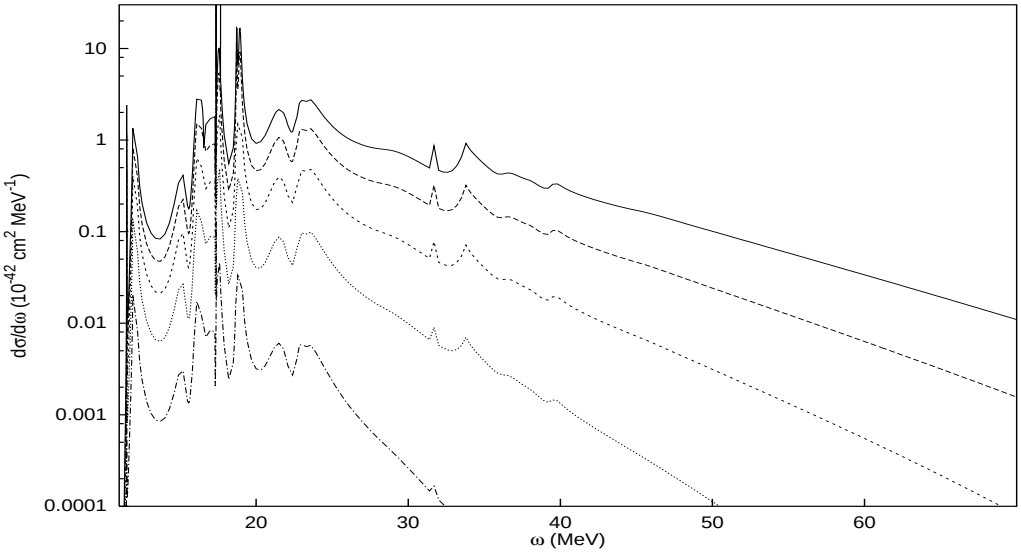


FIG. 9. Differential cross-section for the reaction $^{16}O + \nu_{FD} \rightarrow {}^{16}O^* + \nu'$, averaged over neutrinos and antineutrinos and over a Fermi-Dirac distribution with temperature T. T=12 MeV (full line) ; T=10 MeV (dashed) ; T=8 MeV (shortdashed) ; T=6 MeV (dotted) and T=4 MeV (dashed-dotted).

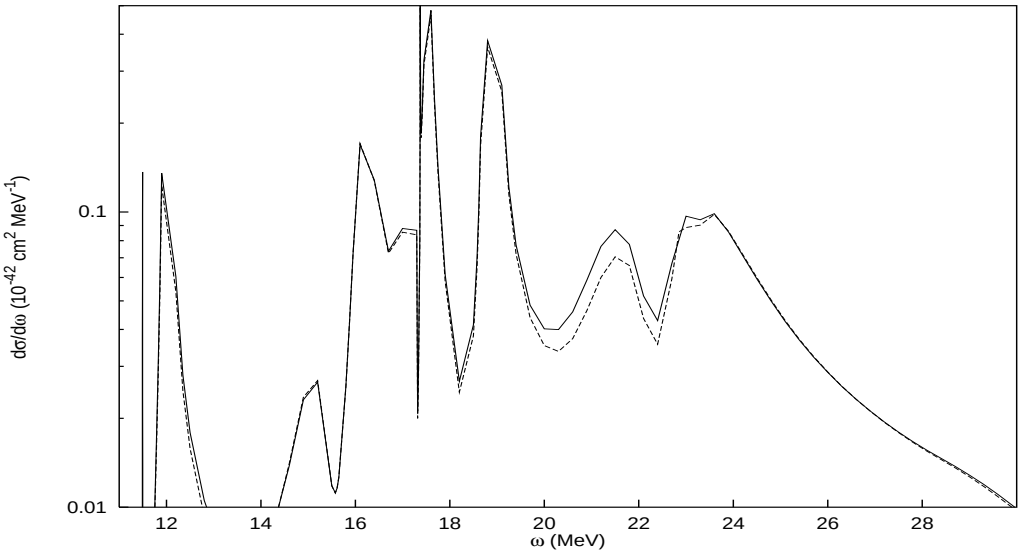


FIG. 10. Differential cross-section for the reaction $^{16}O + \nu_{FD} \rightarrow {}^{16}O^* + \nu'$, averaged over neutrinos and antineutrinos and over a Fermi-Dirac distribution with temperature T=6 MeV, $\alpha$=0 (full line) and $\alpha$=5 (dashed).

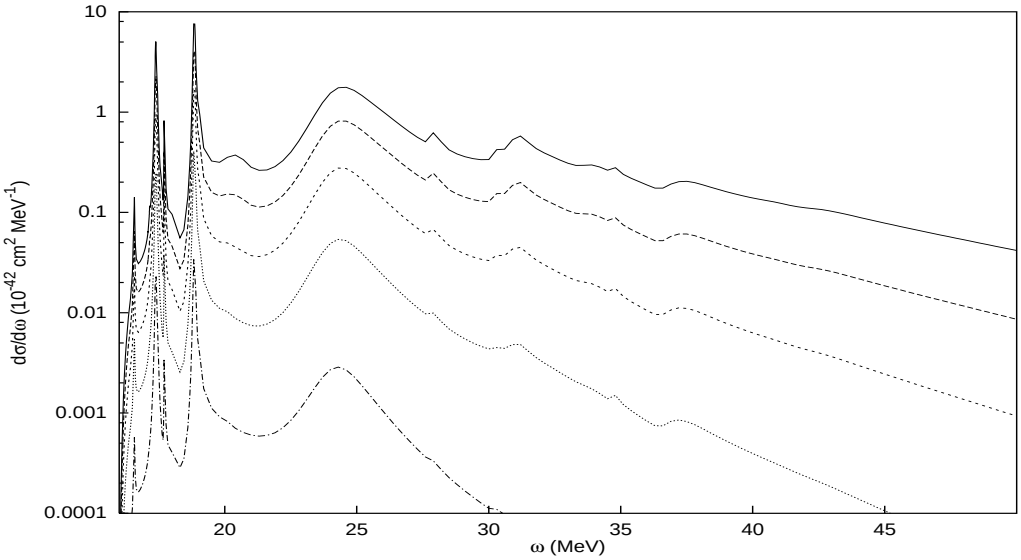


FIG. 11. Differential cross-section for the reaction $^{12}C + \nu_{FD} \rightarrow {}^{12}C^* + \nu'$, averaged over neutrinos and antineutrinos and over a Fermi-Dirac distribution with temperature T. T=12 MeV (full line) ; T=10 MeV (dashed) ; T=8 MeV (shortdashed) ; T=6 MeV (dotted) and T=4 MeV (dashed-dotted).

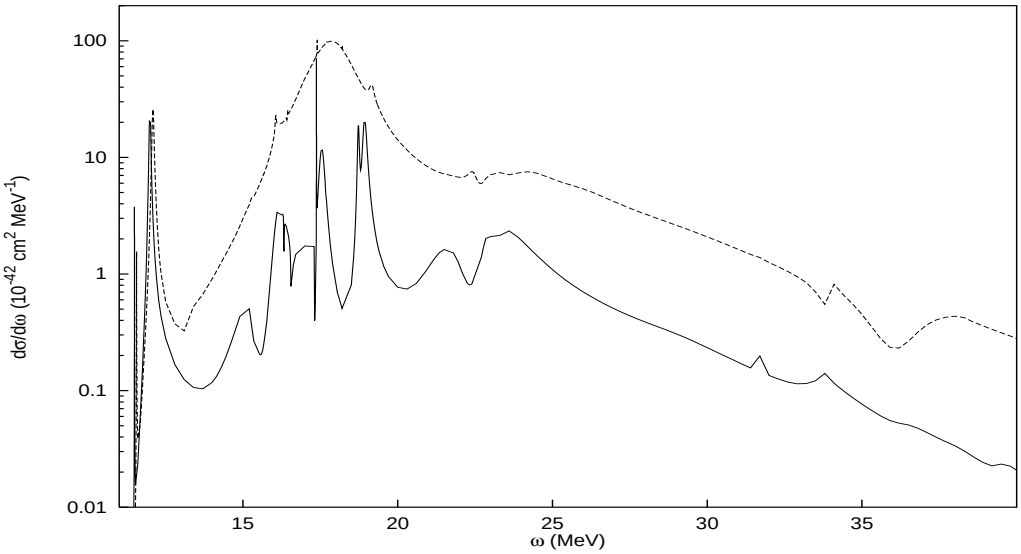


FIG. 12. Comparison of RPA (full line) to TDA results (dashed) for the reaction $^{16}O(\nu,\nu')^{16}O^*$. The discrepancy is most pronounced in the $J^\pi = 1^+$, $2^-$ and $0^+$ channels. The incoming neutrino energy is 50 MeV. All multipoles up to J=4 are taken into account.

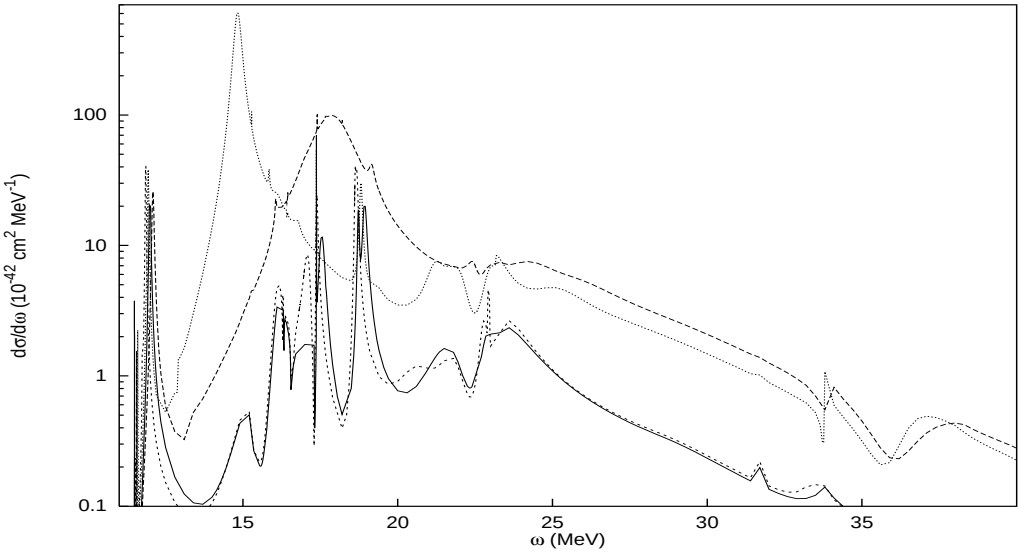


FIG. 13. Comparison of the dependence of RPA and TDA results on the residual interaction used. Whereas RPA calculations are stable against changes in the interaction, TDA cross-sections are not. RPA-SkE2 (full line) ; RPA-LM (shortdashed) ; TDA-SkE2 (dashed) ; TDA-LM (dotted).

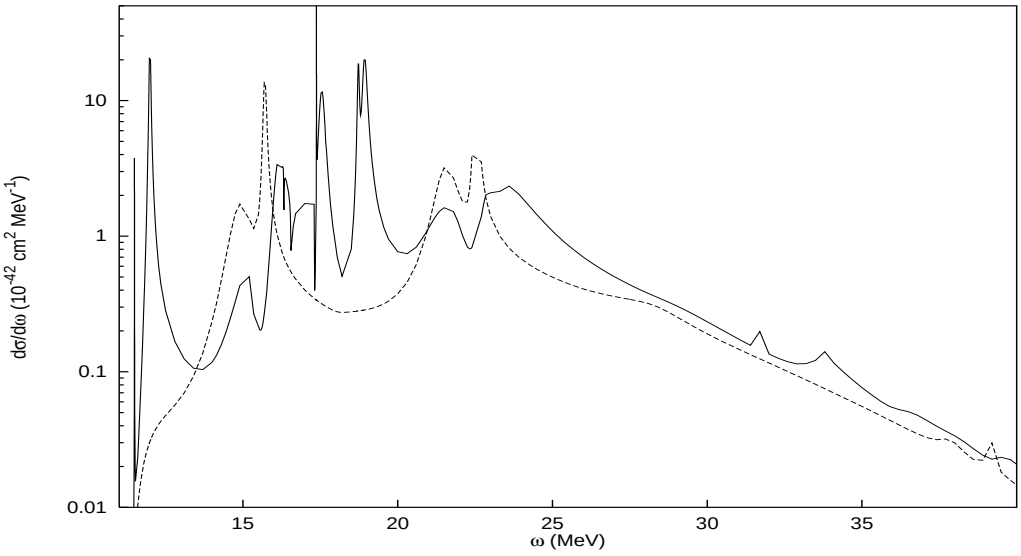


FIG. 14. Comparison of RPA (full line) to Hartree-Fock (dashed) results. The incoming neutrino energy is 50 MeV. All multipoles up to J=4 are taken into account. The large difference between the random phase and the mean-field response at low excitation energies indicates that RPA calculations in this energy region may not give as accurate a description as one could expect. For excitation energies above $\sim$ 27 MeV, RPA calculations provide a reasonable correction to the mean-field ones.